ACS APPLIED MATERIALS & INTERFACES

Research Article

www.acsami.org

Heteroepitaxy of Tetragonal $BiFeO_3$ on Hexagonal Sapphire(0001)

Y. J. Zhao,[†] Z. G. Yin,*[,†] X. W. Zhang,*[,†] Z. Fu,[†] B. J. Sun,[‡] J. X. Wang,[‡] and J. L. Wu[†]

[†]Key Lab of Semiconductor Materials Science and [‡]State Key Laboratory of Solid-State Lighting, Institute of Semiconductors, Chinese Academy of Sciences, Beijing 100083, People's Republic of China

Supporting Information

ABSTRACT: Highly elongated $BiFeO_3$ is epitaxially grown on hexagonal sapphire(0001) substrate within a rather narrow synthesis window. Both X-ray reciprocal space maps and Raman characterizations reveal that it is of true tetragonal symmetry but not the commonly observed M_C type monoclinic structure. The tetragonal $BiFeO_3$ film exhibits an island growth mode, with the island edges oriented parallel to the ⟨10−10⟩ and ⟨12−30⟩ directions of the sapphire substrate. With increasing deposition time, a transition from square island to elongated island and then to a continuous film is observed. The metastable tetragonal phase can remain on the substrate without relaxation to the thermally stable rhombohedral phase up to a critical thickness of 450 nm, providing an exciting opportunity for practicable lead-free ferroelectrics. These results facilitate a better understanding of the phase stability of $BiFeO_3$ polymorphs and enrich the knowledge about the heteroepitaxial growth mechanism of functional oxides on symmetry-mismatched substrates.

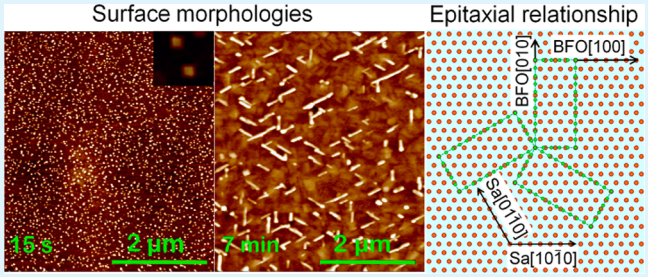

KEYWORDS: *heteroepitaxy, bismuth ferrite, metastable phase, island growth*

I. INTRODUCTION

Heteroepitaxy provides an extra freedom to modify the structures and therefore to control or even create new functionalities of transition-metal oxides through strain engineering.[1−3] A representative example is $BiFeO_3$ (BFO), a room-temperature multiferroic that has attracted considerable research interest in recent years. The fairly strong coupling between ferroelectric and antiferromagnetic orderings makes it possible to control magnetization electrically, or vice versa, thereby opening up prospects for novel spintronic devices.[4,5] Under low and moderate compressive epitaxial strains, the crystal symmetry of the BFO film is lowered from rhombohedral (R) $R3c$ in its bulk form to the monoclinically distorted M_A structure (following the notation of Vanderbilt and Cohen[6]).[7] Accompanied with this symmetry change, a polarization rotation from [111] toward the [001] pseudocubic crystallographic direction and a notable reduction of the Curie temperature occur.[8,9] The epitaxial strain also leads to depression of the long-range cycloidal magnetic modulation superimposed on the antiferromagnetic order.[10] The manipulation of ferroic properties through heteroepitaxy has profound implications for the design of magnetoelectric and magnonic devices.[9,11]

Besides the ground-state $R3c$ structure of BFO, a $P4mm$ tetragonal (T) phase with a large c/a ratio of 1.27 has been theoretically predicted.[12] Along with the huge elongation of the c-axis lattice constant, the six-coordinated FeO_6 octahedron is anticipated to be replaced by a FeO_5 pyramid in the BFO lattice.[13,14] This drastic change in the crystal structure has a strong impact on the ferroic properties: it leads to an unprecedentedly enhanced polarization (~150 $\mu C/cm^2$) and a hugely reduced antiferromagnetic Neel temperature.[12,15] Recent experimental studies have indeed corroborated the existence of such a highly elongated structure via heteroepitaxial growth of BFO on substrates with a large lattice misfit (exceeding -4%).[16,17] However, careful structural examinations revealed that it is not of $P4mm$ symmetry but has a monoclinic M_C structure.[18] This observation is in good accordance with first-principles calculations, which show that the monoclinic structure is energetically more stable than the tetragonal one.[19] Very recently, monoclinic−tetragonal transitions were observed at elevated temperatures, suggesting that the tetragonal phase is the high-temperature form of the M_C structure.[20,21] Besides the temperature, it was suggested that the misfit strain can also induce the M_C-to-tetragonal symmetry change.[22] The tetragonal phase was observed at room temperature by chemical alloying with barium, based on which a compressive strain-mediated R−M_A (R-like)−M_C−T phase transition path was proposed.[22] On the other hand, Fu et al. found that the tetragonal phase can serve as a structural bridge between the M_C-BFO and the heavily strained R-like phase.[23] However, phase-pure, true tetragonal BFO (T-BFO) without chemical doping has not yet been realized at room temperature, and the understanding of such a phase is still limited.

In this paper, we report the epitaxial growth of T-BFO, rather than the M_C structure, on hexagonal sapphire(0001) substrate. A rather narrow growth window was revealed, and the epitaxial relationships were clarified. Unlike the layer-by-layer growth

Received: November 14, 2013
Accepted: January 27, 2014
Published: January 27, 2014

mechanism for M_C-BFO films deposited on perovskite-like substrates, *T*-BFO exhibits an island growth mode. We observed a unique surface morphology evolution from square island to elongated island and finally to a continuous film. The *T*-BFO epilayer can remain on a sapphire of up to a thickness of 450 nm, much higher than the critical thickness reported for M_C-BFO films. The thermal mismatch between the epilayer and substrate is invoked to explain the occurrence of *T*-BFO at room temperature.

II. EXPERIMENTAL PROCEDURE

The BFO films were fabricated by radio-frequency magnetron sputtering on sapphire(0001) substrates. The BFO target was prepared by compressing the ground Bi_2O_3 and Fe_2O_3 powder mixture (with a molar ratio of 1.05:1) into a 80-mm-diameter copper cup. The BFO powder target was used without any high-temperature sintering to suppress severe bismuth evaporation. Prior to deposition, the sputtering chamber was evacuated to a base pressure of 5×10^{-5} Pa and then filled with the working gas of argon and oxygen. The partial pressures of argon and oxygen were set as 0.3 and 0−0.5 Pa, respectively, yielding a total working pressure of 0.3−0.8 Pa. The substrate temperature ranges from 550 to 750 °C. The growth rate at 650 °C and an oxygen partial pressure of 0.2 Pa was determined to be ∼180 nm/h.

Room-temperature X-ray diffraction (XRD) $2\theta-\theta$ and Φ scans were recorded by Rigaku D/MAX-2500 system using Cu Kα as the X-ray source. Temperature-dependent XRD measurements were performed by the Panalytical X'pert Pro setup. Reciprocal space maps (RSMs) were collected by a high-resolution Bede D1 diffractometer with an X-ray wavelength of 1.54056 Å, and the results were shown as plots of the intensity with respect to q in the reciprocal lattice unit, where $q = \lambda/2d$. Surface morphologies were characterized by atomic force microscopy (AFM) by a NT-MDT solver P47 under semicontact mode. Raman scattering experiments were carried out in backscattering geometry by a Horiba LabRAM HR800 spectrometer using excitation line λ = 514 nm of an argon-ion laser.

III. RESULTS

A. Epitaxial Growth of BFO on Sapphire(0001). Figure 1 shows the XRD $2\theta-\theta$ curves of BFO films prepared at different substrate temperatures. Apart from the sapphire peaks, strong (001) reflection of Bi_2O_3 is observed at 550 °C. A small amount of *T*-like BFO coexists with Bi_2O_3 at 550 °C, and its reflection intensities increase sharply with increasing the growth temperature to 600 °C. Besides the (00*l*) peaks, no other BFO-related reflections were observed in the curve, suggesting perfect *c*-axis orientation of the film [BFO(001)‖sapphire(0001)]. The derived *c*-axis cell parameter is ∼4.65 Å, similar to that of the M_C-BFO reported in the literature.[17,18] The Bi_2O_3 impurity phase is unstable at high temperatures,[24] and only *T*-like BFO remains at 650 °C and above. The temperature-dependent evolution of BFO and Bi_2O_3 found here agrees well with the observation in the *R*-like BFO case.[24] The crystal quality of BFO is somewhat deteriorated with increasing growth temperature from 700 to 750 °C, as evidenced by the notable broadening of the full width at half-maximum of the BFO(00*l*) reflections. Moreover, low oxygen partial pressure (<0.1 Pa) induces the occurrence of impurity phases, while high oxygen partial pressure (>0.3 Pa) leads to the formation of the *R*-like phase (see the Supporting Information). Combined with these results, we conclude that phase-pure *T*-like BFO is favored in a growth window with a deposition temperature in the vicinity of 650−700 °C and an oxygen pressure near 0.1−0.3 Pa. Such a rather narrow window explains why the reported attempts to synthesize BFO on sapphire(0001) only led to the formation of polycrystalline *R*-like phases.[25,26]

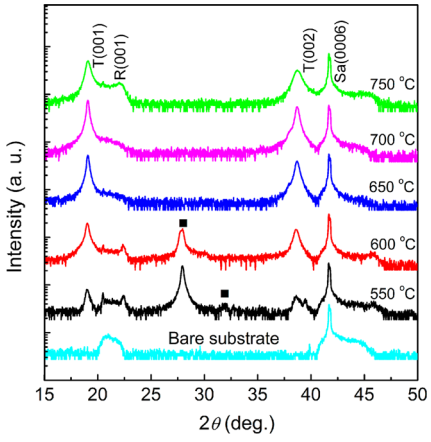

Figure 1. XRD $2\theta-\theta$ scans of the BFO films deposited at various temperatures on sapphire(0001) substrates with a growth time of 20 min. Solid squares (■) denote the reflections from the Bi_2O_3 impurity phase.

To reveal the in-plane orientation of *T*-like BFO with respect to the sapphire substrate, XRD Φ scans were collected along the BFO(101) and sapphire(11-26) reflections for the samples grown at 650 and 700 °C (Figure 2a,b). A total of 12 well-defined BFO(101) peaks were clearly resolved for the 700 °C film. Six of them occur at azimuthal angles identical with those of sapphire(11-26), while the others are shifted 30° from the substrate peaks. Taking into account the fourfold symmetry of BFO(001) and sixfold symmetry of sapphire(0001), the corresponding in-plane epitaxial relationship between BFO and the substrate is derived as follows: BFO[100]‖sapphire[10-10] and BFO[010]‖sapphire[12-30] (type I). Moreover, 12 extra weak peaks shifted ∼±15° from the positions of sapphire(11-26) were observed in the Φ scan curve of the 650 °C film, indicating another in-plane epitaxial relationship: BFO[100]‖sapphire[5-2-30] and BFO[010]‖sapphire[34-70] (type II). Each type of epitaxial relationship results in three equivalent families of domains with an in-plane rotation of 120° from each other (Figure 2c,d). These relationships make it possible to epitaxially grow *T*-like BFO on the hexagonal sapphire(0001) surface.

We note that the in-plane lattice constants of sapphire and BFO are 4.76 and 3.77 Å (as discussed later), respectively, giving rise to a lattice misfit as high as ∼20%. However, the misfit largely reduces to 1% and 0.6% along the [100] and [010] crystallographic directions of BFO, respectively, once considering a 5 × 11 supercell of type I configuration, as illustrated in Figure 2c. Similarly, by taking into account a 8 × 9 supercell, the type II epitaxial relationship yields lattice misfits of 1.44% and 1.15% along the BFO[100] and [010] directions (Figure 2d). Apparently, the type I domains are energetically more favorable because of the smaller supercell size and lower lattice misfit. Therefore, both the 650 and 700 °C films are dominated by type I domains. At elevated temperatures, the surface diffusion rate is much enhanced and thus the deposited atoms have more chances to be captured in the energetically preferred type I configuration. As a result, the XRD reflections from the type II domains are weakened with increasing substrate temperature and are not resolved for the 700 °C film (Figure 2a). The growth of the BFO epilayer is dependent on

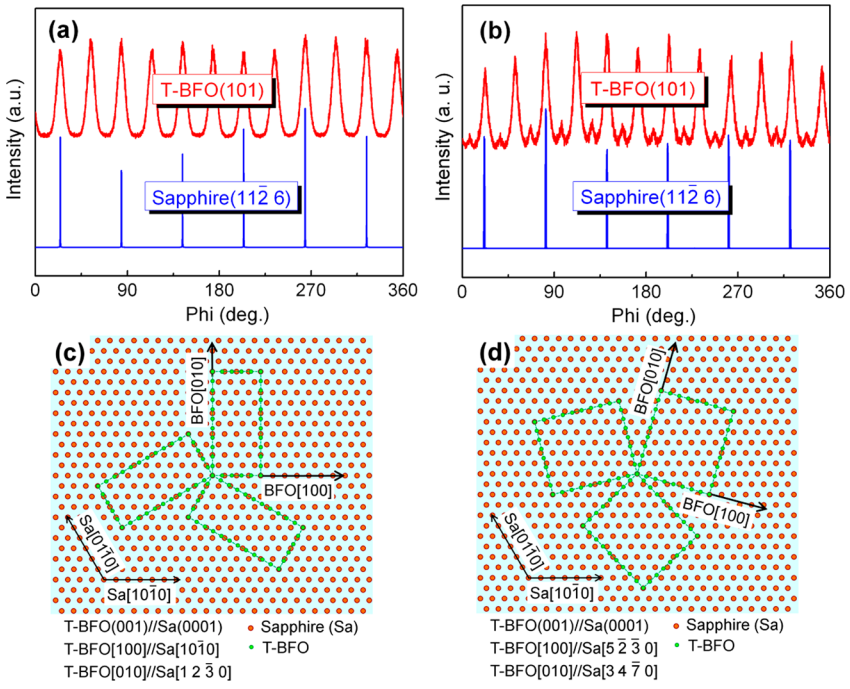

Figure 2. XRD Φ scans of BFO(101) and sapphire(11-26) reflections for the 60-nm-thick films grown at 700 °C (a) and 650 °C (b). Schematic illustrations of types I (c) and II (d) heteroepitaxial relationships between the BFO layer and the sapphire(0001) substrate.

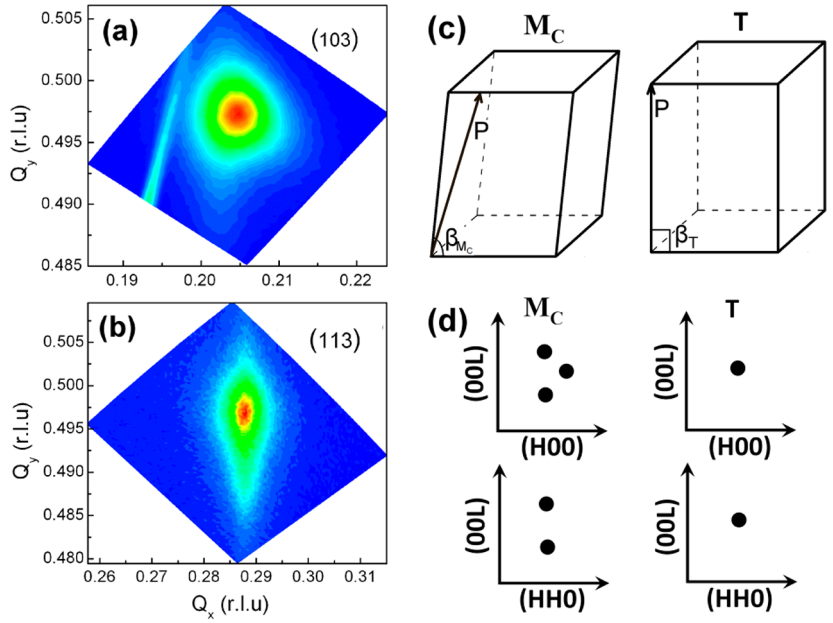

Figure 3. RSMs collected around (103) (a) and (113) (b) reflections of the 60-nm-thick BFO film deposited at 650 °C. (c) Schematics of primitive unit cells of the M_C and tetragonal structures, in which the arrows denote the spontaneous polarization vectors. (d) Representations of the (*H*0*L*) and (*HHL*) planes of the M_C and tetragonal structures in the reciprocal space.

the competition and delicate balance of two such types of domains. Our work develops a possible strategy to synthesize (001)-oriented epilayers of perovskite-like functional oxide on symmetry-mismatched substrates.

B. Crystal Symmetry. To reveal the detailed structure of the BFO epilayer, RSMs around the (103) and (113) reflections were collected, and the results are shown in Figure 3a,b. No measurable peak splitting was observed in either (103) or (113) RSMs, indicating a tetragonal rather than monoclinic M_C structure of the BFO layer.[18] Figure 3c illustrates the primitive unit cells of the tetragonal and M_C structures, and the respective representations of the (*H*0*L*) and (*HHL*) planes in the reciprocal space are shown in Figure 3d. Apparently, the M_C structure yields threefold and twofold splitting for the (*H*0*L*) and (*HHL*) reflections, whereas no splitting occurs for the tetragonal phase. The lattice parameters extracted from the patterns in Figure 3a,b are $a = b = 3.77$ Å and $c = 4.65$ Å. The derived c/a ratio (1.23) and unit cell volume (66.13 Å^3) are all close to those of the M_C phase, consistent with theoretical predictions.[19] The finding of the tetragonal phase on

dx.doi.org/10.1021/am405115y | ACS Appl. Mater. Interfaces 2014, 6, 2639−2646

sapphire(0001) is in marked contrast to the observation of monoclinic M_C-BFO on perovskite-like substrates such as $LaAlO_3$ and $YAlO_3$.[18,20]

To further explore the crystal symmetry of the BFO epilayer deposited on sapphire(0001), Raman characterization was performed on the 60-nm-thick film, and the result is shown as curve a in Figure 4. For comparison, we also display the

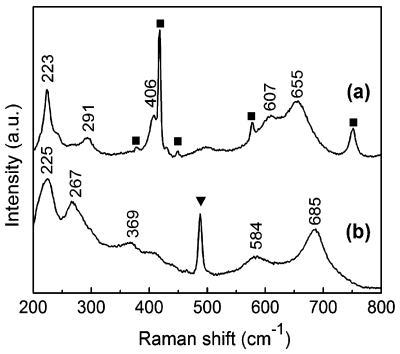

Figure 4. Raman spectra recorded on BFO/sapphire(0001) (a) and BFO/$LaAlO_3$(001) (b) heterostructures deposited at 650 °C. Solid squares (■) and triangles (▲) denote peaks of the sapphire and $LaAlO_3$ substrates, respectively.

Raman spectrum of the BFO film grown on the $LaAlO_3$(001) substrate (curve b). These two spectra are quite distinct from each other. The curve obtained from BFO/$LaAlO_3$ is in good accordance with the observations in the literature,[27,28] indicative of a monoclinic distorted M_C structure of the film. The spectrum collected on BFO/sapphire does not match any of the available experimental results for the known phases, including M_C-BFO, the R phase, and its stress-distorted versions, but is in qualitative agreement with the theory predictions for the $P4mm$ tetragonal structure.[29] According to Raman selecting rules, $P4mm$ symmetry yields eight Raman-active modes ($3A_1 + B_1 + 4E$).[27,28] However, for the (001)-oriented film, the E modes are forbidden and only four Raman lines ($3A_1 + B_1$) are observable under the backscattering geometry. On the basis of first-principles calculations performed by Tutuncu and Srivastava,[29] the peaks located at 223, 406, and 655 cm^{-1} are assigned to A_1 modes, while the signal at 291 cm^{-1} is ascribed as the B_1 line of the T-BFO phase. The extra peak occurring at 607 cm^{-1} possibly originated from the E mode due to symmetry broken at the BFO island surface or from the minority of the M_A (tetragonal-like) phase, one of the low-temperature forms of T-BFO. Although Raman characterization cannot preclude the occurrence of a tiny quantity of other phases, it does provide evidence that the BFO epitaxial films grown on sapphire(0001) are mainly composed of the tetragonal phase, in agreement with the RSM results.

C. Growth Mechanism and Thickness-Dependent Structural Evolution. Figure 5 shows the deposition-time-dependent surface morphology evolution of the T-BFO samples. Deposition of 15 s under 650 °C and an oxygen partial pressure of 0.2 Pa leads to the formation of uniformly distributed islands on the substrate surface (Figure 5a). The inset of Figure 5a clearly reveals that these islands are square in shape, with a lateral dimension of ∼40 nm and a height of ∼3 nm. The edges of the islands are oriented parallel to the ⟨10-10⟩ and ⟨12-30⟩ directions of sapphire, further evidencing the epitaxial relationship between T-BFO and the substrate shown in Figure 2. The island growth mode observed here is at odds with the layer-by-layer mechanism for BFO films deposited on perovskite-like substrates.[30] As the growth time rises to 45 s, rectangular islands due to anisotropic growth were clearly observed on the surface (Figure 5b). Further increasing the deposition time to 3.5 min greatly enhances the island length but has little influence on the width (Figure 5c). The average island length, width, and height for the 3.5 min sample are 400, 70, and 12 nm, respectively. Although the lengths are different from island to island, the widths are quite similar, in good accordance with the theoretical results.[31] According to the calculations performed by Tersoff and Tromp,[31] the trade-off between surface (interface) and elastic energies determines a critical island dimension α_0; beyond α_0, the square shape becomes unstable and a transition from square to elongated islands occurs. During elongation of the islands, their widths

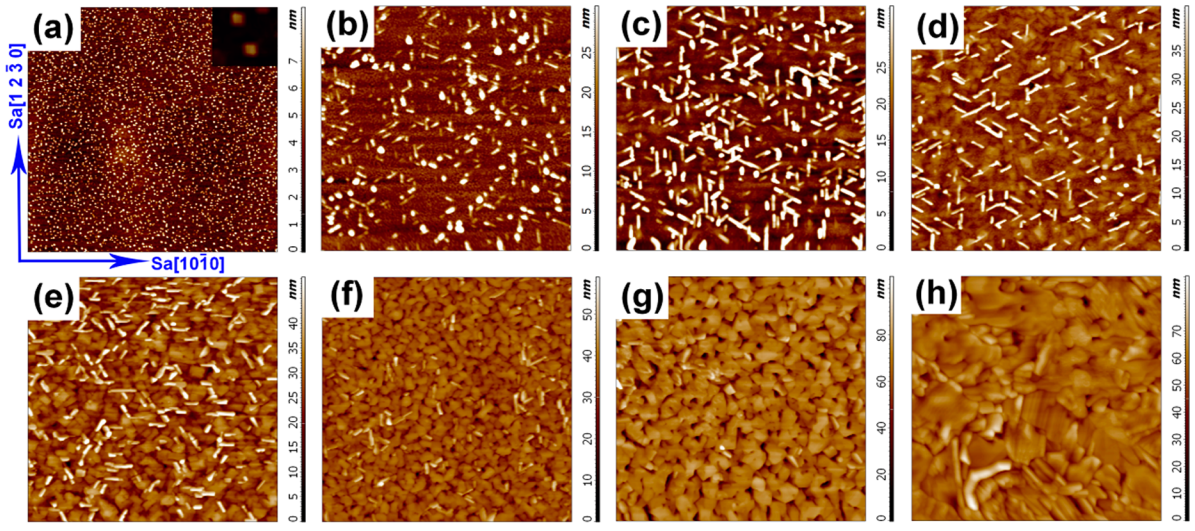

Figure 5. AFM morphologies of BFO samples with deposition times of 15 s (a), 45 s (b), 3.5 min (c), 7 min (d), 20 min (e), 40 min (f), 1 h (g), and 3.5 h (h). A deposition-time-dependent surface morphology evolution from square to elongated islands and finally to a continuous film is demonstrated. The inset of part a shows that the islands at their initial growth stage are square in shape with edges parallel to the ⟨10-10⟩ and ⟨12-30⟩ directions of the sapphire.

remain constant at the optimum value of α_0. The critical dimension α_0 of the *T*-BFO island is determined to be ~70 nm. The island elongation is along the ⟨12-30⟩ direction of the sapphire, consistent with the in-plane supercell illustrated in Figure 2c. The coalesced islands constitute a continuous film with increasing deposition times to 7 and 20 min, as illustrated in Figure 5d,e. Moreover, the rectangular islands gradually merge into the film and are almost invisible on the surface of the 40 min sample (Figure 5f). The resultant film is composed of densely packed columns, and the column size increases drastically with the thickness (Figure 5g,h).

Here we strengthen that island elongation is most commonly observed in metal silicides but is rare in metal oxides.[32,33] To the best of our knowledge, the observation presented herein is the only reported case of such an island shape transition in perovskite-like oxides. The elongated BFO islands shown in Figure 5 can be viewed as one-dimensional nanowires because of their rather large aspect ratio (length/width) of ~6. Ferroelectric nanowires exhibit unique physical properties such as strong magnetoelectric coupling, depression of the phase transition temperature, and tunable remanent polarization and dielectric permittivity and have potential applications in nanoscale electromechanical devices, nonvolatile ferroelectric random-access memory, and advanced sensors.[34] Chemical routes are widely used to synthesize one-dimensional ferroelectric nanostructures while physical methods have scarcely been reported.[35−37] The island shape transition shown in our work demonstrates a possible bottom-up physical approach to the self-assembly of single-crystalline ferroelectric nanowires. Our method has the advantages of cost-effectiveness, ease of fabrication, and good control of the orientation and radial size of the nanowires. However, the aspect ratio of our BFO nanowires is still quite limited. More work is being done in our laboratory concerning the manipulation of the aspect ratio by tuning the growth parameters, such as the deposition rate, sputtering pressure, and substrate temperature, and the results will be reported in due course.

Tetragonal BFO is a pseudomorph of the *R* phase stabilized by heteroepitaxy. It is inherently unstable and, therefore, a relaxation from *T*-BFO to the energetically more favorable *R* phase is expected with increasing film thickness. We note that the pseudomorphic phase transformation route is at odds with the classical interfacial dislocation-mediated stress relaxation mechanism and usually results in a very large critical thickness.[38] For instance, the M_C-BFO film deposited on perovskite-like substrates starts to relieve its stress at a thickness of tens of nanometers.[30] The *T*-BFO phase obtained here can even be retained on sapphire(001) without relaxation up to a thickness of 450 nm (Figure 6), 1 order of magnitude larger than that of the M_C-BFO case. Such a rather thick *T*-BFO film has important implications for both fundamental physics and future applications.[39] When the epilayer thickness reaches 630 nm, a bulklike *R* phase starts to appear to coexist with the *T*-BFO matrix. Upon further increasing thickness to 900 nm, the tetragonal phase almost fully transforms into *R*-BFO. Reflections of (111) and (-111) are present accompanied with the *T*−*R* transition, indicating the occurrence of epitaxy breakdown of the film. No evidence of triclinic or monoclinic M_I phase, which bridges the M_C−*R* transition,[30] was found in our films, contrary to the observationns for M_C-BFO grown on $LaAlO_3$ (see the Supporting Information). This observation reveals that *T*-BFO exhibits a thickness-dependent lattice relaxation process quite different from that of M_C-BFO. This is

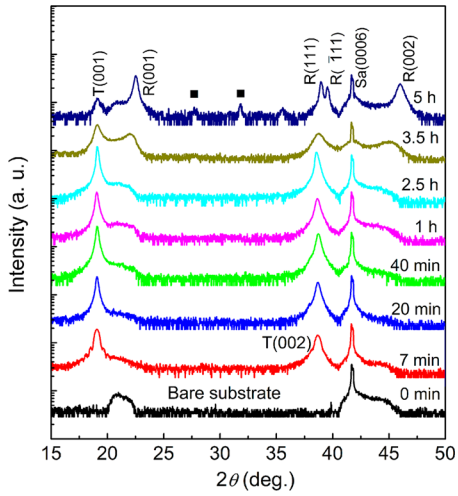

Figure 6. Deposition-time-dependent XRD 2θ−θ scans of BFO films deposited at 650 °C. The growth rate is determined to be ~180 nm/h, and the nominal thicknesses of the films with deposition times of 7 min, 20 min, 40 min, 1 h, 2.5 h, 3.5 h, and 5 h are 21, 60, 120, 180, 450, 630, and 900 nm, respectively.

further evidenced by the surface morphology measurements. When the thickness of M_C-BFO exceeds a threshold value, tilted phases including M_I and $M_{II,tilt}$ appear and form periodic stripelike patches on the film surface (see the Supporting Information). Such a stripelike feature is the fingerprint of stress alleviation of the M_C phase.[30] The lack of these structures in our 630-nm-thick film (Figure 5h) further supports that M_C-BFO is not present on sapphire(0001), in line with the RSMs and Raman results.

Lead-free ferroelectric materials are urgently needed owing to the increasing demands in environmental protection and human health. In the past few years, a variety of materials have been considered as possible candidates to replace lead-based ferroelectrics. *T*-like BFO is one of the most intensively studied because of its largest remanent polarization among all known ferroelectrics. The giant remanent polarization is very promising for reducing the cell size of ferroelectric random access memory (FeRAM) and therefore is of great significance for future applications.[40] However, the nonavailability of a thick *T*-like M_C-BFO film is a bottleneck to its utilization. For instance, on the $LaAlO_3$(001) substrate, the M_C−*R* transition starts at a thickness of 40 nm and completes at 350 nm.[30,41] Our work demonstrates a critical thickness of 450 nm of *T*-BFO on the sapphire substrate and therefore opens up a new avenue for the application of high-performance, lead-free ferroelectrics.

IV. DISCUSSION

A recent study by Diéguez et al. revealed the intrinsic richness of BFO phases and demonstrated that a variety of low-symmetry phases with large *c*/*a* ratios are energetically more stable than the ideal tetragonal *P*4*mm* structure.[19] In fact, the commonly observed supertetragonal BFO films deposited on perovskite-like substrates have a monoclinic M_C structure.[18,30] Very recently, a M_C−M_A−*T* phase transition sequence was clearly observed upon elevation of the temperatures of the films on perovskite-like substrates,[20,21] suggesting that *T*-BFO is the high-temperature form of the M_C phase. For the energetically more favorable M_C-BFO, the constrained polarization in the (010) plane results in anisotropic in-plane lattice parameters (*a*

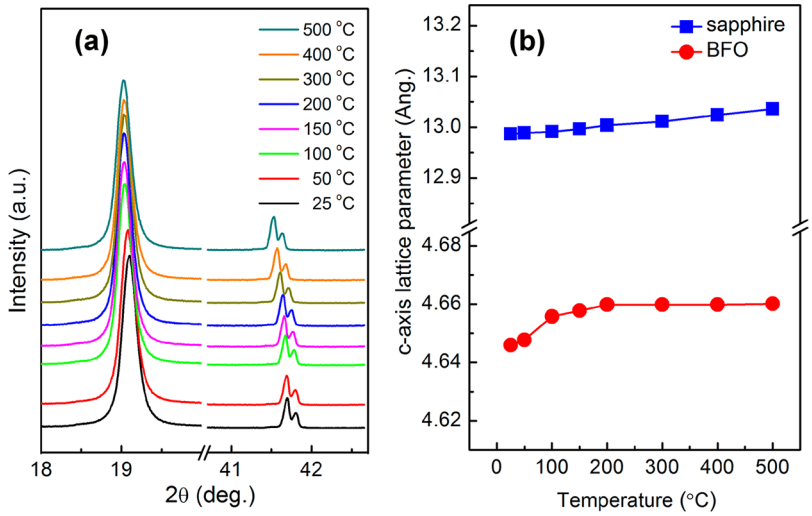

Figure 7. (a) Temperature-dependent XRD $2\theta-\theta$ scans of the 60-nm-thick BFO film grown on sapphire(0001). (b) Derived out-of-plane lattice parameters as a function of the temperature.

= 3.74 Å and b = 3.82 Å).[30] Note that in our case the coherent BFO lattice has tensile and compressive in-plane strain along the ⟨10-10⟩ and ⟨12-30⟩ directions of the sapphire substrate, respectively, again favoring the formation of M_C-BFO rather than the tetragonal phase. However, our results show that the high-temperature, high-symmetry tetragonal phase is stabilized at room temperature.

It is well-known that the lattice misfit determines whether the *R*-like or *T*-like phases are formed on a given substrate.[22] Apparently, *T*-like phases are formed on substrates including sapphire, $LaAlO_3$, and $YAlO_3$. The difference is that a true tetragonal phase is stabilized on sapphire, while BFO is in the monoclinic M_C form on $LaAlO_3$ and $YAlO_3$ at room temperature. However, at growth temperatures of 650−700 °C, BFO exhibits the high-symmetry tetragonal form on all of these substrates.[20,21] Now the question is, why does a tetragonal−monoclinic transition occur on $LaAlO_3$ and $YAlO_3$ but not on sapphire during the cooling process? We note that once the lattice registry of *T*-BFO to the substrate is achieved at the growth temperature, the thermal mismatch plays a key role in modifying its structure by changing the c/a ratio (here a denotes the average in-plane lattice parameter) during the cooling stage. To clarify the influence of thermal mismatch on the tetragonal-phase stabilization on sapphire, we performed temperature-dependent XRD $2\theta-\theta$ scans of the 60-nm-thick film, and the results are shown in Figure 7a. The derived out-of-plane lattice constants, as a function of the temperature, are illustrated in Figure 7b. The out-of-plane lattice of BFO remains constant above 200 °C, in contrast to the observations on $LaAlO_3$ (see the Supporting Information), because of different thermal mismatches. The thermal expansion coefficient in the (0001) plane of sapphire (7.5×10^{-6} K^{-1}) is lower than that in the pseudocubic (001) plane of $LaAlO_3$ (10.8×10^{-6} K^{-1}).[42,43] A rough estimate yields an increase of the c/a ratio by ∼0.5% when BFO/$LaAlO_3$ is cooled from 500 to 200 °C, assuming that the in-plane lattice of the film is clamped to the substrate while out-of-plane relaxation is free. However, on sapphire the increase of c/a during the same process is estimated to be only ∼0.2%. Although the c/a values cannot be precisely determined above 500 °C because of decomposition of BFO during measurements, it is safe to say that variation of the c/a ratio is much larger on $LaAlO_3$ than on sapphire.

Recent works revealed that the c/a ratio is closely related to the detailed crystal symmetry of BFO. When Bi^{3+} (1.38 Å) was replaced with larger-ionic-radius cations, e.g., Ba^{2+} (1.61 Å), a notable decrease of c/a was observed on the $LaAlO_3$ substrate.[44] Along with this c/a ratio reduction, there occurs a M_C-to-tetragonal symmetry change.[22] Akin to this finding, Damodaran et al. demonstrated that the monoclinic distortion angle decreases with a reduction of the c/a value through substitution of a small quantity of Bi^{3+} by Pb^{2+} (1.49 Å).[45] Very recently, Liu et al. found that the monoclinic angle increases with increasing film thickness, accompanied with an enhancement in the c/a ratio.[20] All of these results infer that there exists a threshold of the c/a ratio for the transition between the tetragonal phase and its monoclinic counterpart. Beyond that threshold, BFO exhibits the monoclinic form, and the higher the c/a ratio, the larger the shear distortion.

During the cooling process, the rather small thermal mismatch between BFO and sapphire leads to stabilization of the tetragonal phase, while for BFO on $YAlO_3$ and $LaAlO_3$ substrates,[20,21] the c/a ratio exceeds the threshold during cooling and a transition to the monoclinic phase occurs due to the much larger thermal mismatch. We note that the monoclinic−tetragonal transition temperature of BFO on $LaAlO_3$ is higher than that on $YAlO_3$. This fact further backs up our assumption that thermal mismatch is a key factor that influences the structure of the BFO epilayer, taking into account that $LaAlO_3$(001) has a larger in-plane thermal expansion coefficient than $YAlO_3$(001).[43,46] Although our intuitive explanation imposes a phenomenological connection between the c/a ratio and the structural evolution of the *T*-BFO phase, the underlying physics is not understood as yet and first-principles calculations are strongly encouraged. The influences of the elastic energy, phase boundaries, and domain walls on the tetragonal−monoclinic transition during the cooling process also need to be clarified.

Finally, we turn to the anomaly that occurs at ∼100 °C (Figure 7b). Such an anomaly suggests a discontinuity in the thermal expansion coefficient of BFO and is associated with the second-order antiferromagnetic transition.[47] Similar results are found in M_C-BFO films deposited on fourfold-symmetry substrates, e.g., $LaAlO_3$ (see the Supporting Information). These observations reveal that the tetragonal phase and its low-

symmetry counterpart (M_C-BFO) have similar Neel temperatures, in accordance with recent theoretical predictions.[48] Here we note that the M_C−M_A structural transition cannot account for the anomaly appearing at 100 °C because of the absence of the M_C phase in our films. The occurrence of a magnetic transition in T-BFO near room temperature is significant for its future magnetoelectric and piezomagnetic applications.[15]

V. CONCLUSION

In summary, (001)-oriented T-BFO layers were epitaxially grown on hexagonal sapphire(0001) substrates, in a rather narrow growth window with a substrate temperature in vicinity of 650−700 °C and an oxygen pressure near 0.1−0.3 Pa. The tetragonal symmetry of BFO was corroborated by RSMs and Raman characterization. The predominant in-plane epitaxial relationship between T-BFO and the substrate is BFO[100]||sapphire[10-10] and BFO[010]||sapphire[12-30]. Such findings provide a possible route for synthesizing functional oxides on symmetry-mismatched substrates. The BFO epilayers are formed through a multistep process: square island appearance, square-to-elongated island transformation, island coalescence, and film formation. The observed island shape transition is useful in synthesizing and manipulating BFO low-dimensional nanostructures and exploring their unique properties. Moreover, the tetragonal phase of BFO can stabilize on the sapphire substrate up to a thickness of 450 nm. Such a thick T-BFO film has significant implications for future lead-free ferroelectric applications.

■ ASSOCIATED CONTENT

Supporting Information

Results of XRD analysis of the BFO/sapphire(0001) films deposited at various oxygen partial pressures, XRD and AFM measurements of the 60-nm-thick BFO grown on the $LaAlO_3$(001) substrate, and temperature-dependent XRD characterization of BFO/$LaAlO_3$(001). This material is available free of charge via the Internet at http://pubs.acs.org.

■ AUTHOR INFORMATION

Corresponding Authors

*E-mail: yzhg@semi.ac.cn.
*E-mail: xwzhang@semi.ac.cn.

Author Contributions

The manuscript was written through contributions of all authors. All authors have given approval to the final version of the manuscript.

Notes

The authors declare no competing financial interest.

■ ACKNOWLEDGMENTS

This work was financially supported by the National Natural Science Foundation of China (Grants 11274303 and 51071145), the National Basic Research Program of China (Grant 2012CB934203), and the Knowledge Innovation Program of the Chinese Academy of Sciences under Grant ISCAS2009T03.

■ REFERENCES

(1) Choi, K. J.; Biegalski, M.; Li, Y. L.; Sharan, A.; Schubert, J.; Uecker, R.; Reiche, P.; Chen, Y. B.; Pan, X. Q.; Gopalan, V.; Chen, L. Q.; Schlom, D. G.; Eom, C. B. Enhancement of Ferroelectricity in Strained $BaTiO_3$ Thin Films. *Science* **2004**, *306*, 1005−1009.

(2) Haeni, J. H.; Irvin, P.; Chang, W.; Uecker, R.; Reiche, P.; Li, Y. L.; Choudhury, S.; Tian, W.; Hawley, M. E.; Craigo, B.; Tagantsev, A. K.; Pan, X. Q.; Streiffer, S. K.; Chen, L. Q.; Kirchoefer, S. W.; Levy, J.; Schlom, D. G. Room-Temperature Ferroelectricity in Strained $SrTiO_3$. *Nature* **2004**, *430*, 758−761.

(3) Lee, J. H.; Fang, L.; Vlahos, E.; Ke, X. L.; Jung, Y. W.; Kourkoutis, L. F.; Kim, J. W.; Ryan, P. J.; Heeg, T.; Roeckerath, M.; Goian, V.; Bernhagen, M.; Uecker, R.; Hammel, P. C.; Rabe, K. M.; Kamba, S.; Schubert, J.; Freeland, J. W.; Muller, D. A.; Fennie, C. J.; Schiffer, P.; Gopalan, V.; Johnston-Halperin, E.; Schlom, D. G. A Strong Ferroelectric Ferromagnet Created by Means of Spin−Lattice Coupling. *Nature* **2010**, *466*, 954−958.

(4) Zhao, T.; Scholl, A.; Zavaliche, F.; Lee, K.; Barry, M.; Doran, A.; Cruz, M. P.; Chu, Y. H.; Ederer, C.; Spaldin, N. A.; Das, R. R.; Kim, D. M.; Baek, S. H.; Eom, C. B.; Ramesh, R. Electrical Control of Antiferromagnetic Domains in Multiferroic $BiFeO_3$ Films at Room Temperature. *Nat. Mater.* **2006**, *5*, 823−829.

(5) Catalan, G.; Scott, J. F. Physics and Applications of Bismuth Ferrite. *Adv. Mater.* **2009**, *21*, 2463−2485.

(6) Vanderbilt, D.; Cohen, M. H. Monoclinic and Triclinic Phases in Higher-Order Devonshire Theory. *Phys. Rev. B* **2001**, *63*, 094108.

(7) Toupet, H.; Le Marrec, F.; Lichtensteiger, C.; Dkhil, B.; Karkut, M. G. Evidence for a First-Order Transition from Monoclinic Alpha to Monoclinic Beta Phase in $BiFeO_3$ Thin Films. *Phys. Rev. B* **2010**, *81*, 140101(R).

(8) Jang, H. W.; Baek, S. H.; Ortiz, D.; Folkman, C. M.; Das, R. R.; Chu, Y. H.; Shafer, P.; Zhang, J. X.; Choudhury, S.; Vaithyanathan, V.; Chen, Y. B.; Felker, D. A.; Biegalski, M. D.; Rzchowski, M. S.; Pan, X. Q.; Schlom, D. G.; Chen, L. Q.; Ramesh, R.; Eom, C. B. Strain-Induced Polarization Rotation in Epitaxial (001) $BiFeO_3$ Thin Films. *Phys. Rev. Lett.* **2008**, *101*, 107602.

(9) Infante, I. C.; Lisenkov, S.; Dupe, B.; Bibes, M.; Fusil, S.; Jacquet, E.; Geneste, G.; Petit, S.; Courtial, A.; Juraszek, J.; Bellaiche, L.; Barthelemy, A.; Dkhil, B. Bridging Multiferroic Phase Transitions by Epitaxial Strain in $BiFeO_3$. *Phys. Rev. Lett.* **2010**, *105*, 057601.

(10) Bea, H.; Bibes, M.; Petit, S.; Kreisel, J.; Barthelemy, A. Structural Distortion and Magnetism of $BiFeO_3$ Epitaxial Thin Films: A Raman Spectroscopy and Neutron Diffraction Study. *Philos. Mag. Lett.* **2007**, *87*, 165−174.

(11) Sando, D.; Agbelele, A.; Rahmedov, D.; Liu, J.; Rovillain, P.; Toulouse, C.; Infante, I. C.; Pyatakov, A. P.; Fusil, S.; Jacquet, E.; Carretero, C.; Deranlot, C.; Lisenkov, S.; Wang, D.; Le Breton, J. M.; Cazayous, M.; Sacuto, A.; Juraszek, J.; Zvezdin, A. K.; Bellaiche, L.; Dkhil, B.; Barthelemy, A.; Bibes, M. Crafting the Magnonic and Spintronic Response of $BiFeO_3$ Films by Epitaxial Strain. *Nat. Mater.* **2013**, *12*, 641−646.

(12) Ederer, C.; Spaldin, N. A. Effect of Epitaxial Strain on the Spontaneous Polarization of Thin Film Ferroelectrics. *Phys. Rev. Lett.* **2005**, *95*, 257601.

(13) Ricinschi, D.; Yun, K. Y.; Okuyama, M. A Mechanism for the 150 $\mu C\ cm^{-2}$ Polarization of $BiFeO_3$ Films Based on First-Principles Calculations and New Structural Data. *J. Phys.: Condens. Matter* **2006**, *18*, L97−L105.

(14) Rossell, M. D.; Ermi, R.; Prange, M. P.; Idrobo, J. C.; Luo, W.; Zeches, R. J.; Pantelides, S. T.; Ramesh, R. Atomic Structure of Highly Strained $BiFeO_3$ Thin Films. *Phys. Rev. Lett.* **2012**, *108*, 047601.

(15) Ko, K. T.; Jung, M. H.; He, Q.; Lee, J. H.; Woo, C. S.; Chu, K.; Seidel, J.; Jeon, B. G.; Oh, Y. S.; Kim, K. H.; Liang, W. I.; Chen, H. J.; Chu, Y. H.; Jeong, Y. H.; Ramesh, R.; Park, J. H.; Yang, C. H. Concurrent Transition of Ferroelectric and Magnetic Ordering Near Room Temperature. *Nat. Commun.* **2011**, *2*, 567.

(16) Bea, H.; Dupe, B.; Fusil, S.; Mattana, R.; Jacquet, E.; Warot-Fonrose, B.; Wilhelm, F.; Rogalev, A.; Petit, S.; Cros, V.; Aname, A.; Petroff, F.; Bouzehouane, K.; Geneste, G.; Dkhil, B.; Lisenkov, S.; Ponomareva, I.; Bellaiche, L.; Bibes, M.; Barthelemy, A. Evidence for Room-Temperature Multiferroicity in a Compound with a Giant Axial Ratio. *Phys. Rev. Lett.* **2009**, *102*, 217603.

(17) Zeches, R. J.; Rossell, M. D.; Zhang, J. X.; Hatt, A. J.; He, Q.; Yang, C. H.; Kumar, A.; Wang, C. H.; Melville, A.; Adamo, C.; Sheng,

G.; Chu, Y. H.; Ihlefeld, J. F.; Erni, R.; Ederer, C.; Gopalan, V.; Chen, L. Q.; Schlom, D. G.; Spaldin, N. A.; Martin, L. W.; Ramesh, R. A Strain-Driven Morphotropic Phase Boundary in $BiFeO_3$. *Science* **2009**, *326*, 977−980.
(18) Chen, Z. H.; Luo, Z. L.; Huang, C. W.; Qi, Y. J.; Yang, P.; You, L.; Hu, C. S.; Wu, T.; Wang, J. C.; Gao, C.; Sritharan, T.; Chen, L. Low-Symmetry Monoclinic Phases and Polarization Rotation Path Mediated by Epitaxial Strain in Multiferroic $BiFeO_3$ Thin Films. *Adv. Funct. Mater.* **2011**, *21*, 133−138.
(19) Dupe, D.; Infante, I. C.; Geneste, G.; Janolin, P. E.; Bibes, M.; Barthelemy, A.; Lisenkov, S.; Bellaiche, L.; Ravy, S.; Dkhil, B. Competing Phases in $BiFeO_3$ Thin Films under Compressive Epitaxial Strain. *Phys. Rev. B* **2010**, *81*, 144128.
(20) Liu, H. J.; Chen, H. J.; Liang, W. I.; Liang, C. W.; Lee, H. Y.; Lin, S. J.; Chu, Y. H. Structural Study in Highly Compressed $BiFeO_3$ Epitaxial Thin Films on $YAlO_3$. *J. Appl. Phys.* **2012**, *112*, 052002.
(21) Beekman, C.; Siemons, W.; Ward, T. Z.; Chi, M.; Howe, J.; Biegalski, M. D.; Balke, N.; Maksymovych, P.; Farrar, A. K.; Romero, J. B.; Gao, P.; Pan, X. Q.; Tenne, D. A.; Christen, H. M. Phase Transitions, Phase Coexistence, and Piezoelectric Switching Behavior in Highly Strained $BiFeO_3$ Films. *Adv. Mater.* **2013**, *25*, 5561−5567.
(22) Christen, H. M.; Nam, J. H.; Kim, H. S.; Hatt, A. J.; Spaldin, N. A. Stress-Induced R−M_A−M_C−T Symmetry Changes in $BiFeO_3$ Films. *Phys. Rev. B* **2011**, *83*, 144107.
(23) Fu, Z.; Yin, Z. G.; Chen, N. F.; Zhang, X. W.; Zhao, Y. J.; Bai, Y. M.; Chen, Y.; Wang, H. H.; Zhang, X. L.; Wu, J. L. Tetragonal−Tetragonal−Monoclinic−Rhombohedral Transition: Strain Relaxation of Heavily Compressed $BiFeO_3$ Epitaxial Thin Films. *Appl. Phys. Lett.* **2014**, *104*, 052908.
(24) Bea, H.; Bibes, M.; Barthelemy, A.; Bouzehouane, K.; Jacquet, E.; Khodan, A.; Contour, J. P.; Fusil, S.; Wyczisk, F.; Forget, A.; Lebeugle, D.; Colson, D.; Viret, M. Influence of Parasitic Phases on the Properties of $BiFeO_3$ Epitaxial Thin Films. *Appl. Phys. Lett.* **2005**, *87*, 072508.
(25) Duan, Z. H.; Yu, Q.; Wu, J. D.; Sun, J.; Hu, Z. G.; Chu, J. H. Lattice Dynamics and Dielectric Functions of Multiferroic $BiFeO_3$/c-sapphire Films Determined by Infrared Reflectance Spectra and Temperature-Dependent Raman Scattering. *Thin Solid Films* **2012**, *525*, 188−194.
(26) Lofland, S. E.; McDonald, K. F.; Metting, C. J.; Knoesel, E.; Murakami, M.; Aronova, M. A.; Fujino, S.; Wuttig, M.; Takeuchi, I. Epitaxy, Texturing, and Second-Harmonic Generation in $BiFeO_3$ Thin Films. *Phys. Rev. B* **2006**, *73*, 092408.
(27) Mazumdar, D.; Shelke, V.; Iliev, M.; Jesse, S.; Kumar, A.; Kalinin, S. V.; Baddorf, A. P.; Gupta, A. Nanoscale Switching Characteristics of Nearly Tetragonal $BiFeO_3$ Thin Films. *Nano Lett.* **2010**, *10*, 2555−2561.
(28) Choi, K. Y.; Do, S. H.; Lemmens, P.; Wulferding, D.; Woo, C. S.; Lee, J. H.; Chu, K.; Yang, C. H. Anomalous Low-Energy Phonons in Nearly Tetragonal $BiFeO_3$ Thin Films. *Phys. Rev. B* **2011**, *84*, 132408.
(29) Tutuncu, H. M.; Srivastava, G. P. Electronic Structure and Lattice Dynamical Properties of Different Tetragonal Phases of $BiFeO_3$. *Phys. Rev. B* **2008**, *78*, 235209.
(30) Damodaran, A. R.; Liang, C. W.; He, Q.; Peng, C. Y.; Chang, L.; Chu, Y. H.; Martin, L. W. Nanoscale Structure and Mechanism for Enhanced Electromechanical Response of Highly Strained $BiFeO_3$ Thin Films. *Adv. Mater.* **2011**, *23*, 3170−3175.
(31) Tersoff, J.; Tromp, R. M. Shape Transition in Growth of Strained Islands: Spontaneous Formation of Quantum Wires. *Phys. Rev. Lett.* **1993**, *70*, 2782−2785.
(32) He, Z. A.; Smith, D. J.; Bennett, P. A. Endotaxial Silicide Nanowires. *Phys. Rev. Lett.* **2004**, *93*, 256102.
(33) Zhou, G.; Yang, J. C. Formation of Quasi-One-Dimensional Cu_2O Structures by in situ Oxidation of Cu(100). *Phys. Rev. Lett.* **2002**, *89*, 106101.
(34) Rorvik, P. M.; Grande, T.; Einarsrud, M. A. One-Dimensional Nanostructures of Ferroelectric Perovskites. *Adv. Mater.* **2011**, *23*, 4007−4034.
(35) Xu, G.; Ren, Z.; Du, P.; Weng, W.; Shen, G.; Han, G. Polymer-Assisted Hydrothermal Synthesis of Single-Crystalline Tetragonal Perovskite $PbZr_{0.52}Ti_{0.48}O_3$ Nanowires. *Adv. Mater.* **2005**, *17*, 907−910.
(36) Limmer, S. J.; Seraji, S.; Wu, Y.; Chou, T. P.; Nguyen, C.; Cao, G. Z. Template-Based Growth of Various Oxide Nanorods by Sol−Gel Electrophoresis. *Adv. Funct. Mater.* **2002**, *12*, 59−64.
(37) Macak, J. M.; Zollfrank, C.; Rodriguez, B. J.; Tsuchiya, H.; Alexe, M.; Greil, P.; Schmuki, P. Ordered Ferroelectric Lead Titanate Nanocellular Structure by Conversion of Anodic TiO_2 Nanotubes. *Adv. Mater.* **2009**, *21*, 3121−3125.
(38) Prinz, G. A. Stabilization of bcc Co via Epitaxial Growth on GaAs. *Phys. Rev. Lett.* **1985**, *54*, 1051−1054.
(39) Woo, C. S.; Lee, J. H.; Chu, K.; Jang, B. K.; Kim, Y. B.; Koo, T. Y.; Yang, P.; Qi, Y. J.; Chen, Z. H.; Chen, L.; Choi, H. C.; Shim, J. H.; Yang, C. H. Suppression of Mixed-Phase Areas in Highly Elongated $BiFeO_3$ Thin Films on $NdAlO_3$ Substrates. *Phys. Rev. B* **2012**, *86*, 054417.
(40) Baek, S. H.; Folkman, C. M.; Park, J. W.; Lee, S.; Bark, C. W.; Tybell, T.; Eom, C. B. The Nature of Polarization Fatigue in $BiFeO_3$. *Adv. Mater.* **2011**, *23*, 1621−1625.
(41) Damodaran, A. R.; Lee, S.; Karthik, J.; MacLaren, S.; Martin, L. W. Temperature and Thickness Evolution and Epitaxial Breakdown in Highly Strained $BiFeO_3$ Thin Films. *Phys. Rev. B* **2012**, *85*, 024113.
(42) Vispute, R. D.; Talyansky, V.; Choopun, S.; Sharma, P. R.; Venkatesan, T.; He, M.; Tang, X.; Halpern, J. B.; Spencer, M. G.; Li, Y. X.; Salamanca-Riba, L. G.; Iliadis, A. A.; Jones, K. A. Heteroepitaxy of ZnO on GaN and Its Implications for Fabrication of Hybrid Optoelectronic Devices. *Appl. Phys. Lett.* **1998**, *73*, 348−350.
(43) Chakoumakos, B. C.; Schlom, D. G.; Urbanik, M.; Luine, J. Thermal Expansion of $LaAlO_3$ and $(La,Sr)(Al,Ta)O_3$ Substrate Materials for Superconducting Thin-film Device Applications. *J. Appl. Phys.* **1998**, *83*, 1979−1982.
(44) Bennett, C. J. C.; Kim, H. S.; Varela, M.; Biegalski, M. D.; Kim, D. H.; Norton, D. P.; Meyer, H. M., III; Christen, H. M. Compositional Tuning of the Strain-Induced Structural Phase Transition and of Ferromagnetism in $Bi_{1-x}Ba_xFeO_{3-\delta}$. *J. Mater. Res.* **2011**, *26*, 1326−1331.
(45) Damodaran, A. R.; Breckenfeld, E.; Choquette, A. K.; Martin, L. W. Stabilization of Mixed-Phase Structures in Highly Strained $BiFeO_3$ Thin Films via Chemical-Alloying. *Appl. Phys, Lett.* **2012**, *100*, 082904.
(46) Chaix-Pluchery, O.; Chenevier, B.; Robles, J. J. Anisotropy of Thermal Expansion in $YAlO_3$ and $NdGaO_3$. *Appl. Phys. Lett.* **2005**, *86*, 251911.
(47) Infante, I. C.; Juraszek, J.; Fusil, S.; Dupe, B.; Gemeiner, P.; Dieguez, O.; Pailloux, F.; Jouen, S.; Jacquet, E.; Geneste, G.; Pacaud, J.; Iniguez, J.; Bellaiche, L.; Barthelemy, A.; Dkhil, B.; Bibes, M. Multiferroic Phase Transition near Room Temperature in $BiFeO_3$ Films. *Phys. Rev. Lett.* **2011**, *107*, 237601.
(48) Escorihuela-Sayalero, C.; Dieguez, O.; Iniguez, J. Strain Engineering Magnetic Frustration in Perovskite Oxide Thin Films. *Phys. Rev. Lett.* **2012**, *109*, 247202.